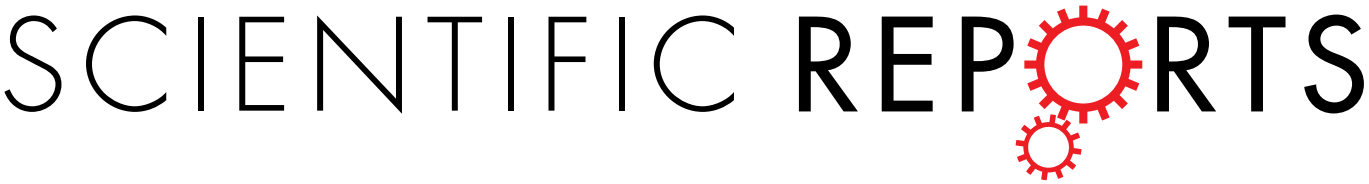

OPEN

Nanostructural origin of blue fluorescence in the mineral karpatite

Received: 9 June 2017
Accepted: 7 August 2017
Published online: 29 August 2017

Jason Potticary[1,2], Torsten T. Jensen[1,3] & Simon R. Hall[1]

The colour of crystals is a function of their atomic structure. In the case of organic crystals, it is the spatial relationships between molecules that determine the colour, so the same molecules in the same arrangement should produce crystals of the same colour, regardless of whether they arise geologically or synthetically. There is a naturally-occurring organic crystal known as karpatite which is prized for its beautiful blue fluorescence under ultra-violet illumination. When grown under laboratory conditions however, the crystals fluoresce with an intense green colour. For 20 years, this difference has been thought to be due to chemical impurities in the laboratory-grown material. Using electron microscopy coupled with fluorescence spectroscopy and X-Ray diffraction, we report here that this disparity is instead due to differences in the structure of the crystals at the nanoscale. The results show that in nature, karpatite has a nanotexture that is not present in the synthetic crystals, which enables different photonic pathways and therefore a blue, rather than green colour whilst undergoing fluorescence.

The optical properties of minerals fundamentally arise from their crystal structure and the spatial arrangement of those crystals across many length scales[1–5]. In the small class of organic hydrocarbon minerals, as is the case in all organic crystals, optical properties are also intimately linked to the relative spatial disposition of molecules within the crystal, with particular polymorphs possessing well-defined optical properties[6–9]. The yellow hydrocarbon mineral karpatite possesses an intriguing property however, in that it fluoresces with a blue colour when illuminated with UV light[10], whereas an optically, chemically and polymorphically identical synthetic analogue (coronene) is green under the same illumination[11]. Here we show through electron microscopy and X-ray crystallography that it is the texturing of karpatite at the nanoscale that is the cause of this blue fluorescence. It was previously thought that the difference in fluorescence behaviour was due to chemical impurities[12], but our data show that this is not the case. Our results reveal that the texturing in karpatite results in self-trapped excitons, giving rise to a dominant absorption band at 460 nm that is not present in coronene. These findings highlight the value of applying a suite of advanced methods in the characterisation of rare minerals, particularly where they possess unexplained physical properties. Our report is the first to identify and ascribe dichotomous colour in organic crystals to morphological variances in the solid-state and furthermore suggest that this phenomenon may be general to many other materials. Indeed, this report unambiguously presents the design motifs that must be present in order to account for unexplained colour differences in any organic crystal.

The mineral karpatite (subsequently - K_P) was first reported in 1955 after being discovered in Zakarpats'ka Oblast in the Ukraine[13]. It is currently known to occur naturally in three locations globally, the Carpathian Mountains, the Tamvatnei mercury deposit in far-east Russia and in San Benito County, CA. in the USA[14]. Historically referred to by a number of names such as 'Pendeltonite', 'Carpathite' and 'Karpatite', it is found as pale-yellow crystalline shards prolifically in cavities between diorite porphyry and argillites (Extended Data Fig. 1). Recent ^{13}C isotopic analysis has suggested that the source material for the mineral is organic matter transported via hydrothermal vents from fault-lines[14]. Karpatite is composed of a crystalline arrangement of molecules of coronene ($C_{24}H_{12}$) a polyaromatic hydrocarbon (PAH). The molecular structure adopted by coronene has the highest thermal stability for any $C_{24}H_{12}$ isomer[13], whose rigidly planar conformation helps fractionate the solubilised coronene into extremely pure nodes by keeping it separate from surrounding impurities[14]. Commercially

[1]Complex Functional Materials Group, School of Chemistry, University of Bristol, Bristol, BS8 1TS, United Kingdom. [2]Bristol Centre for Functional Nanomaterials, HH Wills Physics Laboratory, Tyndall Avenue, Bristol, BS8 1TL, United Kingdom. [3]Centre for Doctoral Training in Condensed Matter Physics, HH Wills Physics Laboratory, Tyndall Avenue, Bristol, BS8 1TL, United Kingdom. Correspondence and requests for materials should be addressed to S.R.H. (email: simon.hall@bristol.ac.uk)

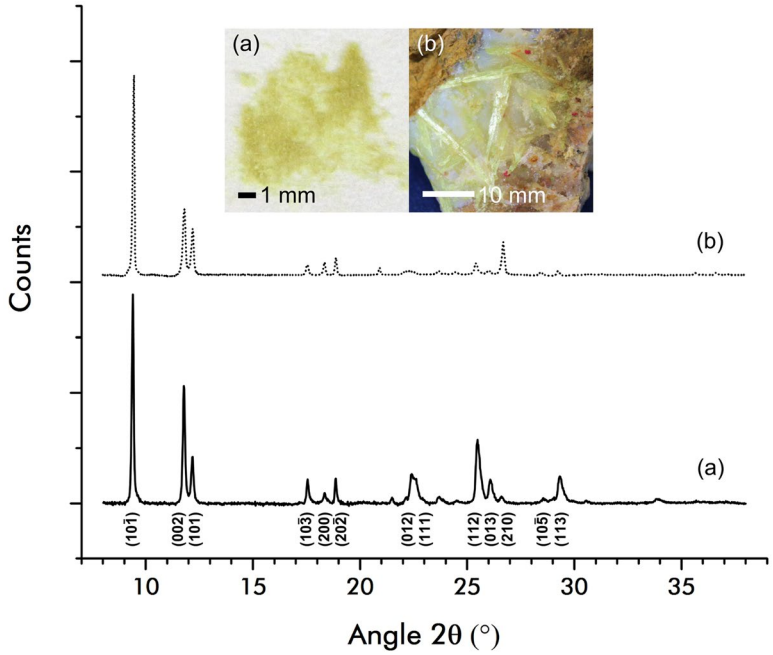

Figure 1. Powder diffraction patterns and images of C_N (solid line) and K_P (dotted line), major reflections have been labelled. Insets show (**a**) powdered recrystallized C_N and (**b**) a vein of K_P (yellow crystals) surrounded by quartz (white crystals) and cinnabar (red spots).

available coronene, once purified by sublimation, can be easily crystallised in the laboratory as acicular yellow crystals (subsequently C_N) which resemble karpatite to the eye.

The crystal structure of both K_P and C_N is due to the fact that the coronene molecule has a large delocalised π-system of sp^2 bonded carbon atoms, with 24 electrons having unimpeded movement around the macro-cycle. This aromaticity lends coronene a rigidly planar conformation within a crystal of which the unit cell is defined as monoclinic, space group $P2_1/n$, parameters $\beta = 106.02°$, $a = 10.122$ Å, $b = 4.694$ Å, $c = 15.718$ Å and $z = 2$[15]. Coronene adopts the γ-herringbone structure according to Desiraju and Gavezzoti's naming convention[16], based on a 4.70 Å short axis and a nearest neighbour stacking angle of 85.01°. The unit cell of K_P was only determined from single crystal data as recent as 2007[14] and was in agreement with data obtained from lab grown crystals. Figure 1 shows powder XRD patterns of both C_N (solid line) and K_P (dotted line) along with optical images for comparison. Both patterns can be indexed to the γ-coronene unit cell with some minor differences in reflection intensity.

Analysis of the pXRD pattern of C_N confirmed the sample as phase pure $P2_1/n$, γ-herringbone crystals (JCPDS card number 12-1611) with little or no amorphous component (Fig. 1 - solid line). Comparison of the K_P pattern with the lab-grown C_N shows a well-matched pattern with regards to the peak positions (Fig. 1 - dotted line). There is, however, a clear difference in peak intensity, implying a difference in texturing between the two samples. Although crushed, orientational effects are still apparent on the intensity profile of the K_P diffraction pattern. Pressing the powder gently onto the XRD sample holder will inevitably cause alignment of the fibres with the substrate.

Historically, the colour of crystallised coronene, whether C_N or K_P, has been described in a variety of ways. Whereas almost all lab-prepared coronene is referred to as having a green appearance under UV illumination, Karpatite has been reported as being 'electric blue' or even 'blue-green'[17] under the same conditions. Although known to be identical chemically and crystallographically, these terms have been used interchangeably throughout the literature, curiously with no distinction or attempt to account for the clear difference in colour between K_P and C_N. Previous investigations on the optical response of PAHs suggest that the cycle stack overlap is the major contributing factor to the strong fluorescence under UV illumination[18]; indeed, recent work would appear to support this claim[19]. However, as polymorph dependant variations in fluorescence are, by definition, restricted to changes in the fundamental unit cell of the PAH, differences between two materials that share the same crystal structure such as K_P and C_N crystals cannot be explained this way. As photon emission and reabsorption is a well-known phenomenon in PAH crystals[20], here we identify and quantify the difference in the optical behavior of C_N and K_P as being the result of macro-structural differences in the two crystalline forms, enabling quite distinct emission and reabsorption pathways.

Optical microscopy of C_N reveals high aspect-ratio needles with parallel sides and truncated ends, consistent with the monoclinic γ-polymorph known to show favourable growth along the short, *b*-axis. When viewed under a polarised-light microscope, parallel extinction was observed indicating that each needle was indeed a single crystal. In order to determine crystallite structure and shape, scanning electron microscopy was used. Figure 2(a) and (b) show starkly that K_P possesses a fibrous/layered structure, with layers having a thickness of ~100 nm.

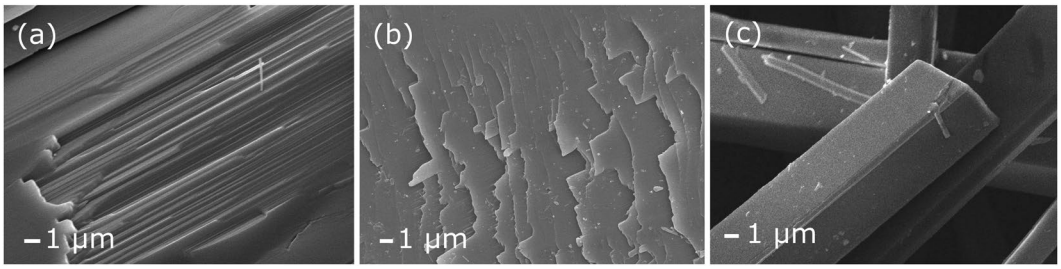

Figure 2. SEM micrographs of native K_P and C_N purified by sublimation. (**a**) Detail of the broken karpatite surface and (**b**) the layering of karpatite exposed at the end of the layered structure. (**c**) An image of a lab grown C_N viewed at the same magnification.

These layers can be seen clearly throughout the entire sample. Figure 2(b) shows an image of the end of a fibre as the layers cause it to taper off. In contrast, Fig. 2(c) shows an SEM micrograph of C_N at the same magnification with no layering visible and no fraying of needle ends. These high-aspect ratio needles have polygonal-defined cross-sections and crystal faces appear smooth and edges are angular.

Single crystal X-ray diffraction of C_N confirms the unit cell was monoclinic with space group $P2_1/n$ as expected. Unit cell parameters were $\beta = 106.29°$, $a = 10.03$ Å, $b = 4.68$ Å, $c = 15.58$ Å and $z = 2$. Stacking distance was calculated to be 3.38 Å. In addition, it is determined that the major growth direction of the C_N needles is also along the short, *b*-axis (Fig. 3).

In order to determine the molecular absorbance of both forms, UV-vis absorption measurements were taken of both types of crystal after dissolution in toluene (Extended Data Fig. 2). Both C_N and K_P produced results that were indistinguishable from each other after a background of pure solvent was subtracted. Absorbance peaks at 341 nm, 326 nm, 305 nm and 293 nm agree with the literature values for coronene[21,22]. Having concordant data between coronene and karpatite in solution confirms that molecularly, the two materials are identical. It is in the solid state, therefore, that we must look to uncover the cause of the materials' differing properties. As stated above, after being illuminated with UV light, K_P emits a brilliant blue colour (Fig. 4(d)), whilst C_N appears green in colour under the same conditions (Fig. 4(c)).

Although coronene has been shown to emit at different wavelengths previously, this is only in solution and bound to other materials[22]. As C_N and K_P are chemically and crystallographically identical, this implies that the difference in the solid state UV response must result from the observed differences in the macroscopic structure (Fig. 2). To measure the difference in UV response quantitatively, both C_N and K_P were analysed via UV-vis spectrophotometry in reflectance mode. For diffuse reflectance measurements, the samples were scanned over the range 800 to 240 nm. Extended Data Fig. 3 shows both the raw diffuse reflectance as a function of λ and the analogous absorbance calculated using the Kubelka-Munk[23] function plotted against energy. The polycrystalline nature of the materials does not allow for a direct comparison of the relative intensities via diffuse reflectance measurement, however it can clearly be seen that the responses of both solids are plainly dissimilar, as evidenced from the starkly different lineshapes. In the case of K_P (dashed line), reflectance begins to drop sharply at 471 nm to 22% at 432 nm. In C_N however, there is a much more gradual decrease in reflectance from 792 nm to 467 nm. Both samples display a similar reflectance from 432 nm to 230 nm with slight differences between 432 nm and 361 nm. The optical band gap for C_N here is calculated as 2.403 eV, which matches closely the literature value of 2.41 eV.[24] In contrast, K_P shows an optical band gap of 2.743 eV, a difference of 0.340 eV from the lab-grown crystal of C_N. Figure 4(a) and (b) show the excitation and emission profiles of both C_N and K_P. The emission profiles for each crystal are markedly different. K_P has a maximum emission at 462.3 nm which is in the blue region of visible light, whereas C_N, has emissions at 501.5 nm and 512.2 nm which is deep within the green. The excitation profile of K_P, for an emission of 462.3 nm, increases fairly evenly with wavelength until 433.0 nm is reached, at which point it sharply drops away. Across the same range, C_N with an emission at 501.5 nm resembles the lineshape for K_P until, unlike K_P, the intensity diminishes. The excitation profile keeps rising until 440.1 nm where it drops again before rising to its maximum intensity at 466.4 nm. It is important to note, upon analysis of these results, intense peaks in the excitation of C_N at 466.4 nm and the emission by K_P at 462.3 nm are of similar shape at a similar wavelength. An energy of 2.66 eV −2.68 eV (466 nm −462 nm) is being emitted from the layered crystal of K_P but not the non-layered C_N. If this layering in K_P is the fundamental cause of the differences in the emission profiles, it would therefore naturally be expected that K_P crystals without this nano-texture would emit in the green wavelength region. To determine if this was indeed the case and to rule out the role of any potential polyaromatic impurities, some K_P was dissolved in toluene, after confirmation of its expected blue emission, and recrystallized by slow evaporation. The resulting crystals were prismatic and indiscernible from C_N via SEM and fluorescence spectroscopy (Extended Data Fig. 4). Furthermore, sublimation of K_P crystals resulted in the deposition of crystals in the cooler region of the tube that exhibited a fluorescence spectroscopy profile similar to K_P crystals, but with the addition of peaks in the C_N-like green region of the emission spectrum at 463, 482 and 527 nm (Extended Data Fig. 5). This would suggest that the sublimation resulted in a mixture of layered and non-layered morphologies, which indeed was the case, as evidenced by SEM images of the sublimed crystals. (Extended Data Fig. 6). These data confirm that the discrete nano-texturing of K_P is the most likely cause of the blue fluorescence. In order to confirm this, we need to consider what mechanism is giving rise to the blue fluorescence in K_P, with the goal of determining how charge transport differs between K_P and C_N. As non-charged molecules, excitonic charge

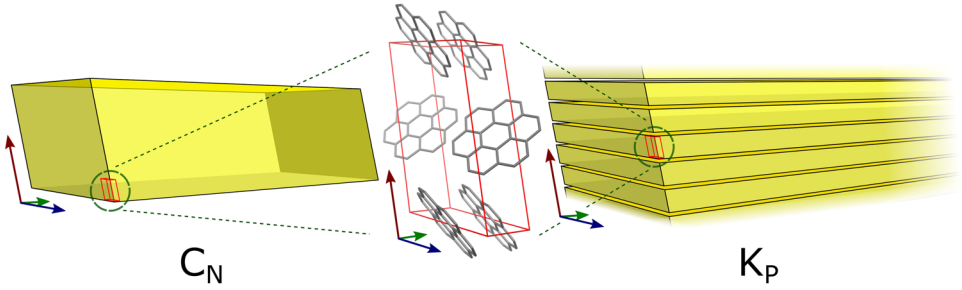

Figure 3. Orientation of the p21/n unit cell of coronene in both C_N (left) and K_P (right). Blue, green and red arrows represent the *a*-, *b*- and *c*-axis directions respectively.

transfer between molecules in PAH crystals, is known to occur along the π-stack, which in the case of C_N is typically the *b*-direction, along the length of the needle[25,26]. It has previously been calculated that this charge transfer between coronene molecules requires 2.68 eV[24] which is extremely close to the 2.66 eV measured experimentally in K_P via UV-vis (the location of the similar band in Fig. 4 mentioned earlier, 2.66–2.68 eV). If charge transfer is indeed causing this optical difference between K_P and C_N, then it is clear that the K_P *c*-axis (corresponding to the thickness of the layers in K_P), must also be the primary route for this 2.66 eV charge transfer, as this is not a route available in C_N due to the lack of nano-texturing in C_N. It follows that electron hopping in K_P involves a significant fraction of movement across the stacks, via edge-face interactions. Another way of confirming that charge transfer excitons are responsible for the colour change is to look at the spectral response of thin (approximately 1 μm thickness) plate-like C_N crystals. Previous studies have shown that these thin C_N crystals do indeed possess a similar spectrum to that seen in K_P sample, with the dominant absorption band at approximately 460 nm in K_P and thin C_N attributed to the presence of self-trapped excitons[12,27]. Calculations performed by Shinozuka and Toyozawa of the relaxed state energy of one, two and three-dimensional organic crystals indicate that, for an infinite three-dimensional crystal lattice, the free exciton state is stable, with a large potential barrier preventing the transition to the trapped state. However, with a finite number of lattice sites and reduced dimensionality, the free state possesses higher energy and thus a free exciton is more likely to transition to the lower-energy self-trapped state[28]. Hence, it appears that the lack of this band in C_N crystals is due to the greater potential barrier separating the free and self-trapped exciton states, compared to that in nanotextured K_P crystals. In contrast to other organic crystals, coronene possesses a deeper self-trapped state[29], which is why it an ideal model for studying the effects of morphological change on the alteration of excitonic luminescence.

In conclusion, we have determined that despite being compositionally identical, lab-grown crystalline coronene and naturally-occurring karpatite exhibit different fluorescence profiles due to nano-texturing of karpatite. Furthermore, we have shown that it is the alteration of the charge transfer mechanism that is concomitant with this texturing that explains the change in fluorescence. Our findings show that through the application of a suite of advanced analytical techniques, a new and deeper understanding of the physical behaviour of rare minerals with unexplained properties can be achieved. As this study represents the first proof that colour change in organic crystals can be a solid-state morphological phenomenon, we believe that our interrogative method can be applied to many other organic crystal systems to potentially uncover exotic charge transfer pathways in semiconductors, field-effect transistors and organic superconductors.

Methods

Crystal Preparation. Coronene (C_N) was synthesised using (97%) purchased from Sigma-Aldrich UK and twice purified by sublimation under vacuum after recrystallization from toluene. The resulting crystals were yellow needles of various lengths up to a maximum of 5 mm. The naturally formed karpatite was reclaimed by gentle excavation of the soft crystalline region, embedded in surrounding quartz, using a PTFE coated spatula to avoid metallic contamination. The pale-yellow flakes were separated from any debris under an optical microscope, no further purification was performed.

Crystallography. Powder x-ray diffraction (pXRD) data were gathered using a Bruker D8 Advance diffractometer (Cu-Kα radiation - wavelength of 1.5418 Å) with a PSD LynxEye Detector. Step size was 0.0411 2θ and hold time was 1.5 s. Both C_N and K_P were only subject to a gentle crushing prior to analysis. Both samples were mounted on a low-background sample holder with silicon wafer.

UV-vis spectroscopy. UV-vis spectroscopy was taken using a Perkin-Elmer Lambda 25 UV/vis spectrophotometer. Samples in solution were dissolved at a known concentration, and dispensed into a 1 cm path-length, quartz cuvette and tested for absorbance between 280 and 360 nm. UV reflectance was obtained in the solid state by mounting the crystalline sample on a barium sulphate substrate behind a quartz window. Using $BaSO_4$ as a reference, the diffuse reflectance of the sample was recorded. This reflectance was converted to analogous solid absorption using the Kubelka-Munk function[11].

Fluorescence spectroscopy. Measurements were obtained after mounting crystalline samples on the end of a quartz plate using paraffin oil. The quartz plate, cut at an 8° angle allowed for emitted light to be detected but

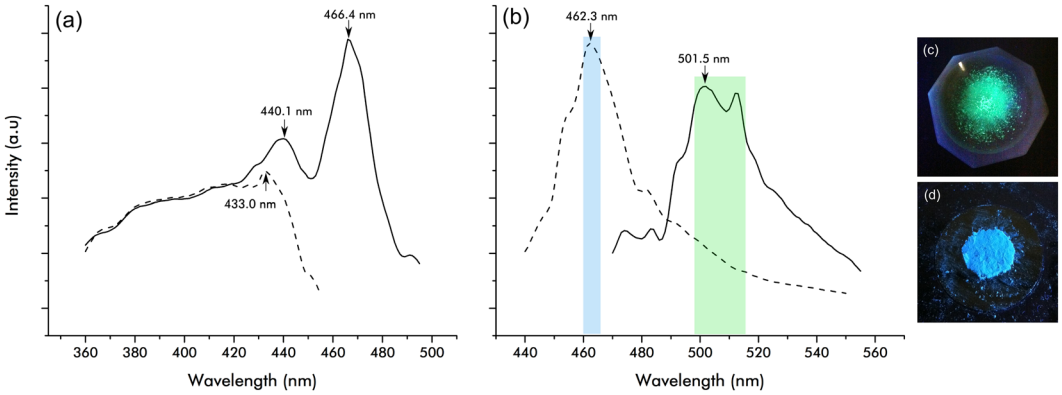

Figure 4. Solid state fluorescence of C_N (solid line) and K_P (dotted line). (**a**) Excitation and (**b**) emission wavelengths were taken using λ_{max} from the corresponding data (C_N ex = 466.4 nm/em = 501.5 nm, K_P ex = 433.0 nm/em = 462.3 nm). The inset images show (**c**) C_N and (**d**) K_P photographed under shortwave UV illumination.

not directly reflect the incident beam. Initial excitation wavelengths were informed by solid state UV-vis results after which emission peaks were identified.

SEM. All Scanning Electron Microscopy (SEM) samples were prepared by mounting on 7 mm aluminium stubs using a sticky carbon pad. These were then sputter coated with a 15 nm of silver. Images were acquired using a JEOL JSM 6330 F high-resolution SEM with a field emission gun and captured using a range of working distances and accelerating voltages.

Data Availability. Data are available at the University of Bristol data repository, data.bris, at https://doi.org/10.5523/bris.3v4w0ka3q7lqg27gznygvh0s02.

References

1. Jansen, M. & Letschert, H. P. Inorganic yellow-red pigments without toxic metals. *Nature* **404**, 980–982 (2000).
2. JoseYacaman, M., Rendon, L., Arenas, J. & Puche, M. C. S. Maya blue paint: An ancient nanostructured material. *Science* **273**, 223–225 (1996).
3. Seitz, F. Color centers in alkali halide crystals. *Rev. Mod. Phys.* **18**, 384–408 (1946).
4. Moore, P. B. Crystal chemistry of the basic iron phosphates. *Am. Mineral.* **55**, 135–169 (1970).
5. Shipman, P., Foster, G. & Schoeninger, M. Burnt Bones and Teeth – An experimental study of color, morphology, crystal structure and shrinkage. *J. Archaeol. Sci.* **11**, 307–325 (1984).
6. Echigo, T. & Kimata, M. Crystal chemistry and genesis of organic minerals: a review of oxalate and polycyclic aromatic hydrocarbon minerals. *Canad. Mineral.* **48**, 1329–1357 (2010).
7. Heinemann, T., Palczynski, K., Dzubiella, J. & Klapp, S. H. L. Coarse-grained electrostatic interactions of coronene: towards the crystalline phase. *J. Chem. Phys.* **143**, 174110 (2015).
8. Chen, S., Guzei, I. A. & Yu, L. New polymorphs of ROY and new record for coexisting polymorphs of solved structures. *J. Am. Chem. Soc.* **27**, 9881–9885 (2005).
9. Wang, H. *et al.* The thermodynamic characteristics of organic crystal growth by physical vapor transport: towards high-quality and color-tunable crystal preparation. *CrystEngComm.* **21**, 4539–4545 (2014).
10. Robbins, M. Fluorescence: gems and minerals under ultraviolet light. Geoscience Press, Phoenix, Arizona, USA. ISBN-10: 0945005-13X (1994).
11. Quin, A. & Tang, B. Z. *Aggregation-induced emission: fundamentals and applications*. John Wiley & Sons, Chichester, UK. ISBN-10: 1118701690 (2014).
12. Matsui, A. H. & Mizuno, K. Crystallization and excitonic luminescence of coronene crystals. *J. Phys. D. Appl. Phys.* **26**, B242–B244 (1999).
13. Piotrovsky, G. L. Karpatite – a new organic mineral from Transcarpathia. *Lvov. geol. Obs. Miner. Sb.* **9**, 120–127 (1955).
14. Echigo, T., Kimata, M. & Maruoka, T. Crystal-chemical and carbon-isotopic characteristics of karpatite ($C_{24}H_{12}$) from the Picacho Peak Area, San Benito County, California: evidences for the hydrothermal formation. *Am. Mineral.* **92**, 1262–1269 (2007).
15. Krygowski, T. & Cyranski, M. Separation of the energetic and geometric contributions to aromaticity. 2. analysis of the aromatic character of benzene rings in their various topological environments in the benzenoid hydrocarbons. Crystal and Molecular Structure of Coronene. *J. Chem. Inf. Comput. Sci.* **2338**, 1135–1141 (1996).
16. Desiraju, G. R. & Gavezzotti, A. Crystal structures of polynuclear aromatic hydrocarbons. Classification, rationalization and prediction from molecular structure. *Acta Crystallogr. Sect. B* **45**, 473–482 (1989).
17. Robbins, M. *The collector's book of fluorescent minerals*. Springer, US. ISBN 978-1-4757-4792-8 (1983).
18. Wang, K. *et al.* Organic polymorphs: one-compound-based crystals with molecular-conformation- and packing-dependent luminescent properties. *Adv. Mater.* **26**, 6168–6173 (2014).
19. Potticary, J. *et al.* An unforeseen polymorph of coronene by the application of magnetic fields during crystal growth. *Nat. Commun.* **7**, 11555 (2016).
20. Powell, R. C. & Soos, Z. G. Singlet exciton energy transfer in organic solids. *J. Lumin.* **11**, 1–45 (1975).
21. Fetzer, J. C. The chemistry and analysis of large PAHs. *Polycycl. Aromat. Compd.* **27**, 143–162 (2007).
22. Dappe, Y. J. & Martínez, J. I. Effect of van der Waals forces on the stacking of coronenes encapsulated in a single-wall carbon nanotube and many-body excitation spectrum. *Carbon NY* **54**, 113–123 (2013).
23. Džimbeg-malčić, V., Barbarić-mikočević, Ž. & Itrić, K. Kubelka-Munk theory in describing optical properties of paper (1). *Tech. Gaz.* **18**, 117–124 (2011).

24. Chen, E. C. M. & Wentworth, W. E. A comparison of experimental determinations of electron affinities of pi charge transfer complex acceptors. *J. Chem. Phys.* **63**, 3183 (1975).
25. Martinelli, N. G. *et al*. Influence of intermolecular vibrations on the electronic coupling in organic semiconductors: the case of anthracene and perfluoropentacene. *ChemPhysChem* **10**, 2265–2273 (2009).
26. Schweicher, G., Olivier, Y., Lemaur, V. & Geerts, Y. H. What currently limits charge carrier mobility in crystals of molecular semiconductors? *Isr. J. Chem.* **54**, 595–620 (2014).
27. Yamamoto, T. *et al*. Exciton-phonon coupling and pressure-induced structural phase changes in coronene crystals. *Chem. Phys.* **184**, 247–254 (1994).
28. Shinozuka, Y. & Toyozawa, Y. Self-trapping in mixed crystal clustering, dimensionality, percolation. *J. Phys. Soc. Japan* **46**, 505–514 (1979).
29. Matsui, A. H. Excitonic processes in aromatic molecular crystals of strong exciton-phonon coupling. *Pure Appl. Chem* **67**, 429–436 (1995).

Acknowledgements

S.R.H., J.P. and T.T.J. acknowledge the Engineering and Physical Sciences Research Council UK (grants EP/G036780/1 and EP/L015544/1), and the Bristol Centre for Functional Nanomaterials and the Centre for Doctoral Training in Condensed Matter Physics for project funding.

Author Contributions

S.R.H. initiated and supervised the project. J.P. performed the crystallisation and structural characterisation experiments at Bristol and characterised the samples optically with T.T.J. All authors contributed to the discussion of the results, analysis of the structures and to manuscript preparation.

Additional Information

Supplementary information accompanies this paper at doi:10.1038/s41598-017-10261-w

Competing Interests: The authors declare that they have no competing interests.

Publisher's note: Springer Nature remains neutral with regard to jurisdictional claims in published maps and institutional affiliations.